Earth and Planetary Science Letters 542 (2020) 116325

Contents lists available at ScienceDirect

Earth and Planetary Science Letters

www.elsevier.com/locate/epsl

Morphometry of a glacier-linked esker in NW Tempe Terra, Mars, and implications for sediment-discharge dynamics of subglacial drainage

Frances E.G. Butcher [a,b,*], Matthew R. Balme [a], Susan J. Conway [c], Colman Gallagher [d,e], Neil S. Arnold [f], Robert D. Storrar [g], Stephen R. Lewis [a], Axel Hagermann [h]

[a] School of Physical Sciences, The Open University, Walton Hall, Milton Keynes, MK7 6AA, UK
[b] Department of Geography, The University of Sheffield, Sheffield, S10 2TN, UK
[c] CNRS, UMR 6112 Laboratoire de Planétologie et Géodynamique, Université de Nantes, France
[d] UCD School of Geography, University College Dublin, Dublin 4, Ireland
[e] UCD Earth Institute, University College Dublin, Dublin 4, Ireland
[f] Scott Polar Research Institute, University of Cambridge, Cambridge, CB2 1ER, UK
[g] Department of the Natural and Built Environment, Faculty of Social Sciences and Humanities, Sheffield Hallam University, Sheffield, S1 1WB, UK
[h] Biological and Environmental Sciences, University of Stirling, Stirling, FK9 4LA, UK

ARTICLE INFO

Article history:
Received 23 September 2019
Received in revised form 5 March 2020
Accepted 4 May 2020
Available online xxxx
Editor: W.B. McKinnon

Keywords:
Mars geomorphology
glaciers on Mars
wet-based glaciation
esker
glacial hydrology

ABSTRACT

We present a systematic, metre-scale characterisation of the 3D morphometry of an esker on Mars, and the first attempt to reconstruct the multi-stage dynamics of esker formation on Mars. Eskers are sinuous ridges comprising sediment deposited by meltwater draining through ice-confined tunnels within or beneath glaciers. Detailed morphometric insights into eskers on Mars are important for (i) informing morphometric tests of whether sinuous ridges elsewhere on Mars are eskers, and (ii) informing modelling experiments which aim to reconstruct the glaciological and environmental controls on esker formation on Mars. We use a digital elevation model generated from High Resolution Imaging Science Experiment (HiRISE) images to characterise the height and width of an extremely rare esker associated with a late-Amazonian-aged viscous flow feature (debris-covered glacier) in NW Tempe Terra, Mars. Our measurements suggest that the NW Tempe Terra esker is a 'stacked' formation comprising an underlying 'lower member' ridge that is superposed by a narrower 'upper member' ridge. We used a novel morphometric approach to test whether the apparent stacking records two distinct esker deposition regimes (either within the same drainage episode, or within temporally-separated drainage episodes). This approach posits that esker crest morphology is controlled by primary esker formation processes and, by extension, that portions of eskers with similar crest morphologies should have similar morphometric relationships. We predicted the morphometric relationships described by the constituent upper and lower member ridges based on 'reference relationships' observed for morphologically-similar portions of the esker where no evidence of stacking was observed. Our observations corresponded well with the predicted relationships, supporting our stacked esker hypothesis. We propose conceptual models, which invoke spatial and temporal variations in sediment supply and meltwater discharge, to explain the stacked morphology. These models are informed by morpho-sedimentary relationships observed along eskers on Earth.

1. Introduction

Sinuous ridge landforms in the Phlegra Montes (162.96°E, 32.68°N; Gallagher and Balme, 2015) and NW Tempe Terra (83.06°W, 46.17°N; Butcher et al., 2017) regions of Mars' northern mid-latitudes have been interpreted as eskers based on their morphologies and associations with glacial landsystems, including extant debris-covered glaciers (viscous flow features, VFF; Gallagher and Balme, 2015; Butcher et al., 2017). Eskers are ridges comprising glaciofluvial sediment deposited in meltwater drainage conduits within or beneath glacial ice. The mid-latitude glacier-linked eskers on Mars indicate that their parent glaciers underwent rare, localised basal melting ~110–150 Ma, despite the extremely cold, arid conditions of the most recent (late Amazonian) period of

* Corresponding author.
E-mail address: f.butcher@sheffield.ac.uk (F.E.G. Butcher).

https://doi.org/10.1016/j.epsl.2020.116325

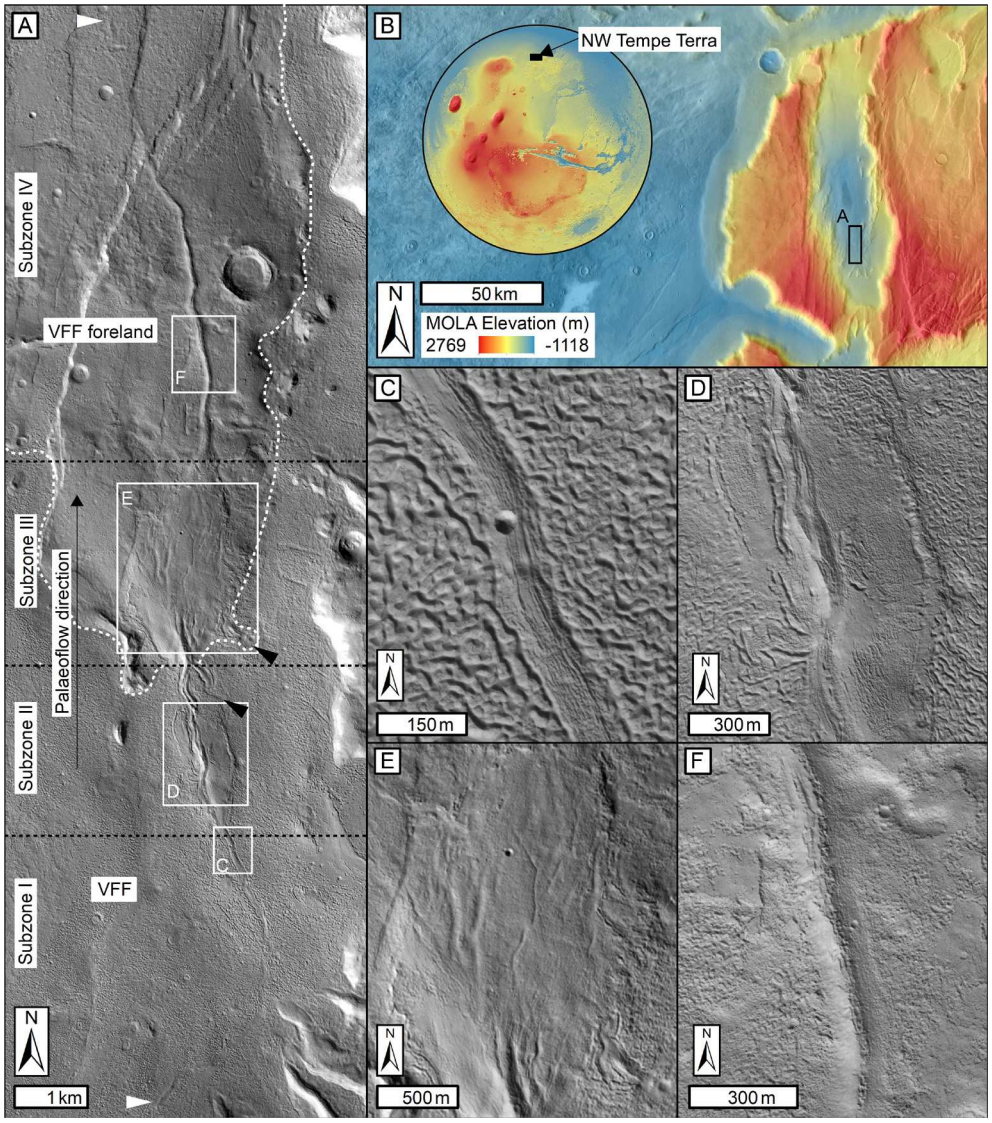

Fig. 1. The glacier-linked esker in NW tempe Terra esker, Mars. (A) Context Camera image mosaic of the glacier-linked esker in NW Tempe Terra. White arrows mark the southern and northernmost visible extent of the esker, black arrows mark heads of two possible tributary eskers, the white dotted line delineates present VFF terminus, black dotted lines delineate morphological subzones I–IV defined by Butcher et al. (2017), and white boxes show extents of panels C–F. Extent shown by black box in panel (B), a colourised Mars Orbiter Laser Altimeter (MOLA) elevation map overlain on Thermal Emission Imaging System Daytime IR image mosaic showing the location of the tectonic rift hosting the glacier-linked esker. Extent shown on inset MOLA elevation globe. Panels C–F show portions of (C) subzone I, (D) subzone II, (E) subzone III, and (F) subzone IV of the esker. Panels C, D and F are orthorectified HiRISE images, and panel C is a CTX image. See Appendix A for list of data products.

Mars' geologic history (Gallagher and Balme, 2015; Butcher et al., 2017). Both eskers are located within tectonic rift/graben valleys. These geologic contexts, combined with the results of modelling experiments, suggest that locally-elevated geothermal heat flux was a pre-requisite for geologically-recent basal melting of glacial ice on Mars (Gallagher and Balme, 2015; Butcher et al., 2017; Arnold et al., 2019; Sori and Bramson, 2019).

In this study, we characterise the metre-scale 3D morphometry of the glacier-linked esker identified by Butcher et al. (2017) in NW Tempe Terra, Mars (83.06°W, 46.17°N; Fig. 1). Our principal aim is to document its morphometry and provide a comparative dataset for future studies aiming to test whether sinuous ridges elsewhere on Mars are eskers. Our raw measurements (Sections 4.1 and 4.2) highlight complexity in the morphology of the NW Tempe Terra esker, and suggest that the ridge is in fact a composite esker formation comprising two 'stacked' ridge members (Section 4.3). We apply a novel morphometric approach to our raw measurements to explore this hypothesis (Section 4.4), and present the morphometries of the constituent ridge members that we identify (Section 4.5). Based on insights from eskers on Earth (Section 5.1; e.g., Banerjee and McDonald, 1975; Brennand, 1994; Burke et al., 2008, 2010, 2012, 2015; Perkins et al., 2016), we then develop conceptual models for the possible sediment-discharge dynamics of meltwater drainage episode(s) that could explain the observed morphometries and esker stacking (Section 5.2).

2. The NW Tempe Terra esker

The glacier-linked esker in NW Tempe Terra (Fig. 1A–B), and its associated landsystem and geologic context, was mapped and described in detail by Butcher et al. (2017). To summarise, the esker emerges from within the tongue of its parent glacier (lobate debris apron-type; e.g., Squyres, 1979), and extends northward into the glacier foreland. It comprises a single trunk ridge system and two short (~400 m long) tributary ridges connecting to its eastern flank. Butcher et al. (2017) defined four major morphological subzones along the esker. Subzone I (~0–5 km; Fig. 1C) is a low-relief, textured band comprising ridges and troughs within the sur-

face of the remnant parent glacier. Subzone II (∼5–8 km; Fig. 1D) comprises a ∼150 m wide, sharp- to multi-crested central prominence atop a broader 500–1500 m wide ridge, the gently-sloping lower flanks of which are mantled by remnant glacier materials of unknown thickness. Subzone III (∼8–11 km; Fig. 1E) is a round-crested ridge portion that is up to 1300 m wide and extends northward into the glacier foreland from the glacier terminus. The ridge narrows gradually towards the subzone III–IV transition. Subzone IV (∼11–17 km; Fig. 1F) has a narrower (150–200 m wide), sharp-crested morphology that extends a further ∼4 km into the glacier foreland. The northernmost ∼2 km of subzone IV comprises fragmented and degraded ridge segments.

3. Data and methods

3.1. Basemap data

We extracted measurements of the esker from the 1 m/pixel digital elevation model (DEM; vertical precision ±0.492 m) and 50 cm/pixel orthorectified images generated by Butcher et al. (2017) from High Resolution Imaging Science Experiment (HiRISE; McEwen et al., 2007) images ESP_049573_2265 and ESP_049639_2265. Given the resolution of the input images, we consider the effective horizontal resolution of the DEM to be 2 m. We imported these data into ESRI ArcGIS 10.1 software in a sinusoidal projection centred on 276.5°E. (the centre of the valley hosting the esker). We then derived slope, shaded relief, and aspect map products from the DEM to aid visual inspection and interpretation of the 3D surface. A list of data products used in this study is provided in Appendix A.

3.2. Measurement of 3D morphometries

Following the methods of Storrar et al. (2014a) and Butcher et al. (2016), we digitised the crests of the individual, unbroken ridge *segments* that form the esker *system* onto the integrated basemap. For the purposes of this study, we digitised only the major trunk system and excluded two ∼400 m long tributary ridges identified by Butcher et al. (2017).

To measure the height and width of the esker, we manually digitised ridge-transverse transects exceeding the ridge width, at 20 m intervals along the esker crestline. We converted each transect to 1 m spaced points and viewed them in topographic profile (with ten times vertical exaggeration) and in planform against the basemap. We classified the left and right ridge base points for each transect as the major breaks in slope either side of the ridge, and the crest as the point of maximum elevation between these points.

Following Butcher et al. (2016), we then calculated ridge height H for each cross-sectional transect as the difference in elevation between the ridge crest point and the bed. We calculated the bed elevation by averaging the elevations of the left and right base points. We calculated ridge width for each cross-sectional transect as the horizontal distance between the right and left base points.

Post-processing of our raw 3D measurements is described in Section 4.4. The crest points and associated raw height and width measurements, in addition to processed height and width data generated during the analyses presented in Sections 4.4 and 4.5, are included in supplementary dataset 1. We performed statistical analyses using R software (R Development Core Team, 2008).

3.3. Sampling

We excluded cross sectional transects from the sample if: (1) the base of the ridge was obscured by proximal tributary ridges, (2) they had been visibly modified by secondary processes such as impact cratering or superposition by moraine ridges (see Butcher et al., 2017), or (3) they were within 40 m of the tapering ends of the ridge segment. We excluded subzone I (Butcher et al., 2017) from our morphometric analyses owing to its near-complete obscuration by superposing VFF materials. Our raw dataset comprised measurements for 457 cross-sectional transects (see Appendix B).

3.4. Measurement uncertainties

Appendix C describes calculations of measurement uncertainties. These uncertainties consider the vertical precision of (±0.5 m), and noise within (±1.3 m), the DEM. We found uncertainties induced by map projection distortion to be insignificant ($\ll$0.001 m). The uncertainties in raw height and width measurements are ±2 m and ±3 m, respectively.

The ridge flanks in subzone II are partially mantled by remnant VFF materials. This probably results in underestimations of ridge dimensions, possibly on the order of tens of metres. The lack of known bed topography prevents quantification of the magnitude of this uncertainty, but a significant break in slope visible at the ridge base points in subzone II suggests that the superposing material is relatively thin; thick ice or ice-rich debris would be expected to have equilibrated this break in slope over time.

4. Results and analysis

4.1. Raw height and width measurements

The distributions of the raw height and width measurements for the NW Tempe Terra esker are shown in Fig. 2A–B. Descriptive statistics for these measurements are displayed in Table D.1 (Appendix D).

When plotted together (Fig. 2C), the raw height and width measurements are positively correlated but exhibit complex trends. Subzone IV measurements follow a simple linear trend, while the subzone II and III measurements exhibit multiple non-linear trends. In the analyses that follow (Sections 4.3 and 4.4), we demonstrate that this complexity is probably an artefact of stacking of two morphologically-distinct esker ridges under a multi-stage deposition regime (Section 5). Hence, the height-width trends illustrated in Fig. 2 and Fig. 3 should not be interpreted as scaling relationships arising from a single, representative regime of meltwater drainage and esker deposition. Instead, simpler height-width trends described by the individual stacked components (extracted in Section 4.4.3), are more likely to reflect their primary deposition regimes.

To simplify our analyses, we exclude transects covering the transitions between morphological subzones (n = 43; crosses in Fig. 2C, see also Appendix B), since their morphometries may not be representative of individual morphological subzones.

4.2. Definition of morphometric domains and their morphologies

Our raw measurements of the NW Tempe Terra esker (Fig. 3) illustrate morphometric complexity below the scale of morphologic subzones I–IV identified by Butcher et al. (2017). We identify six groupings in the scatterplot of raw height and width (Fig. 3), which we term *domains* (coded A–F). As illustrated in Fig. 4, each domain is related to a set of spatially-associated transects along the esker. Five domains (A–E) correspond to transects within subzones II and III. Domain F contains all transects within subzone IV.

Domains A and E have similar height-width trends, while in domains C and D, the ridge is significantly taller for a given width. Domain B exhibits no correlation between raw height and width; transects in this domain cluster in a relatively narrow width range (697–825 m), but their heights (in the range 17–37 m) bridge the gap between transects with similar widths in domains A and E, and C–D.

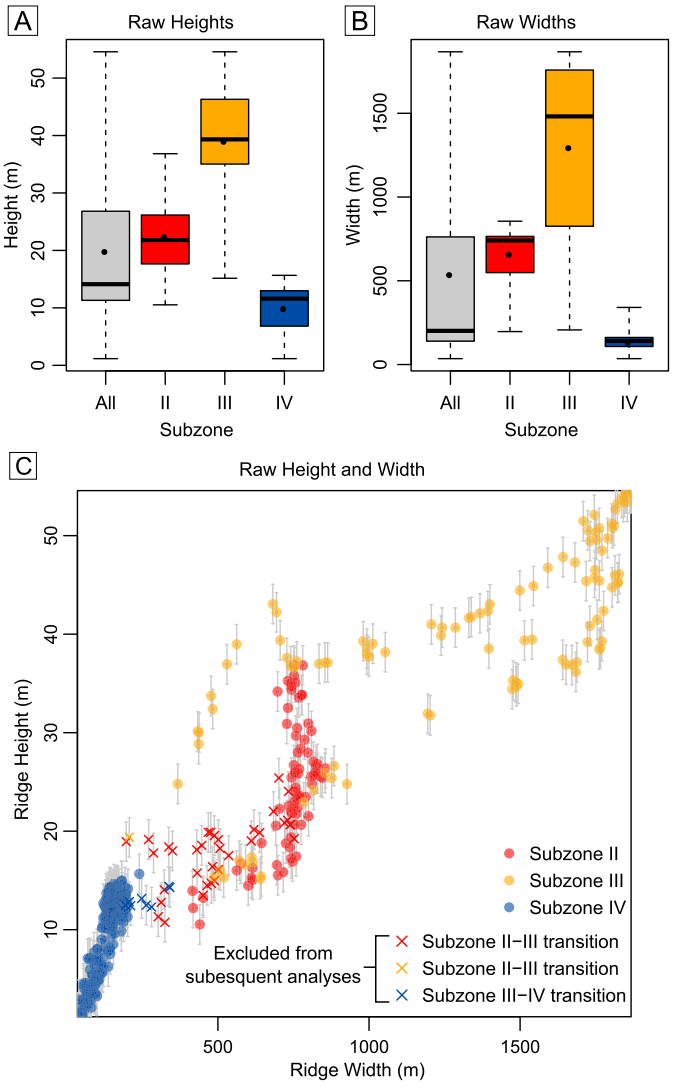

Fig. 2. Distributions of raw height and width measurements along the NW Tempe Terra esker. Panels A–B are boxplots, in which boxes represent the interquartile range, dashed whiskers represent maximum and minimum, solid bars represent the medians, and points represent the means of: (A) raw ridge height, and (B) raw ridge width. Panel (C) is a scatterplot of the raw height and width measurements. Crosses represent transects that occur at transitions between morphological subzones and are excluded from subsequent analyses. Error bars represent uncertainties calculated in Appendix C. In all panels, colours represent subzones defined by Butcher et al. (2017).

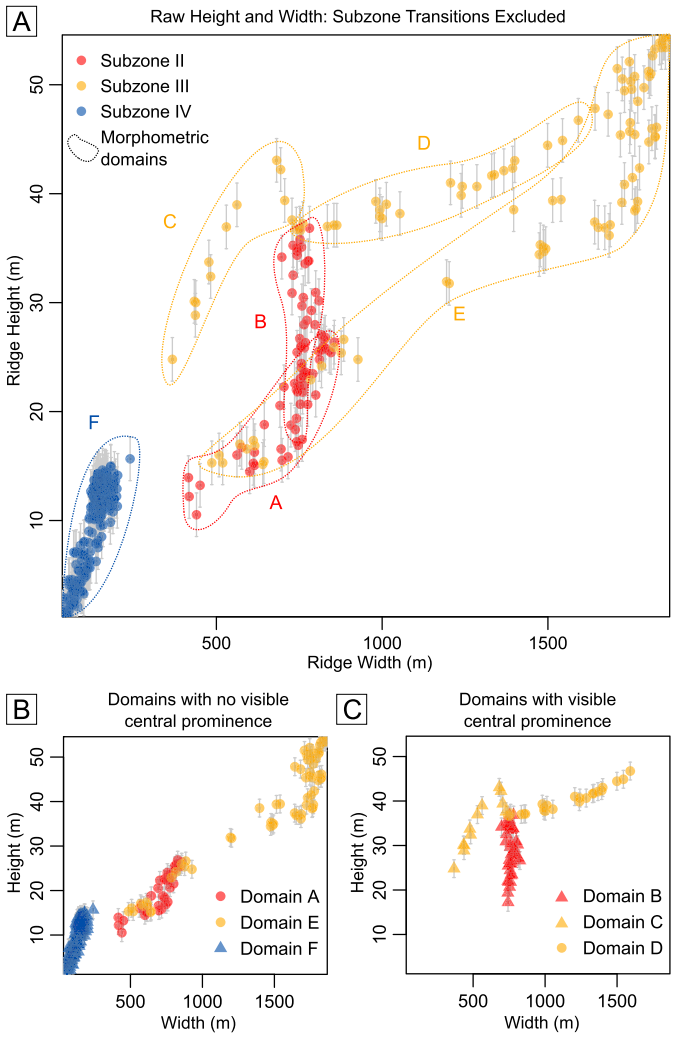

Fig. 3. Definition of morphometric domains along the NW Tempe Terra esker. Scatterplots of raw height and width measurements sampled for further analysis showing: (A) domains of spatially-associated transects (outlined by dotted loops); (B) transects where there is no visible central prominence, which follow two dominant, approximately linear trends; and (C) transects with a visible central prominence. In all panels, error bars represent uncertainties calculated in Appendix C, and colours represent subzones defined by Butcher et al. (2017).

4.2.1. Domains A–B

Domains A–B (Fig. 3) are located in subzone II of the esker (Fig. 4), which Butcher et al. (2017) described as 'multi-crested'. In domain A, the ridge has a broad, rounded central crest, and a second, parallel crest part way down its gently-sloping western flank (Fig. 4B and Fig. 5B–C). The crests are separated by a 100–200 m wide, 2–5 m deep, flat-bottomed trough (Fig. 5B) which is itself partially infilled by a small ridge (Fig. 5C) towards the transition to domain B.

The broad, gently-sloping flanks of domain A continue into domain B (Fig. 4 and Fig. 5D–E). However, the ridge crest in domain B instead has a narrow, more steep-sided central prominence atop the broader ridge (Fig. 5D). The central prominence has a sharp crest which transitions to two sharp, parallel crests which are separated by a 50–60 m wide, ~5 m deep, V-shaped trough.

The central prominence in domain B appears to be continuous with the small ridge that partially infills the northern end of the inter-crest trough in domain A. The sharp to multi-crested central prominence that characterises domain B continues northward to the southern margin of domain C. However, a sampling gap between domains B and C (necessitated by proximity of this portion of the ridge to a possible tributary ridge, see Section 3.3) means that we do not speculate on the morphometry of this ridge portion, despite its morphological similarity to domain B.

4.2.2. Domains C–F

Domain C (Fig. 4) corresponds to a short portion of the ridge extending north from the subzone II–III transition identified by Butcher et al. (2017). It is morphologically similar to domain B (i.e., comprising broad lower flanks and a steep-sided central prominence), except that the central prominence is entirely characterised by a single crest (Fig. 5F). The sharp-crested central prominence gradually becomes lower, wider, and more round-crested (Fig. 5G) into domain D, transitioning to a spatulate form that grades into the surface of the broader ridge at the northernmost end of domain D (Fig. 4).

Domain E has a relatively simple, wide, round-crested morphology (Fig. 4; Fig. 5H), and lacks a central prominence. It narrows and lowers towards its northern end, tapering towards the transition

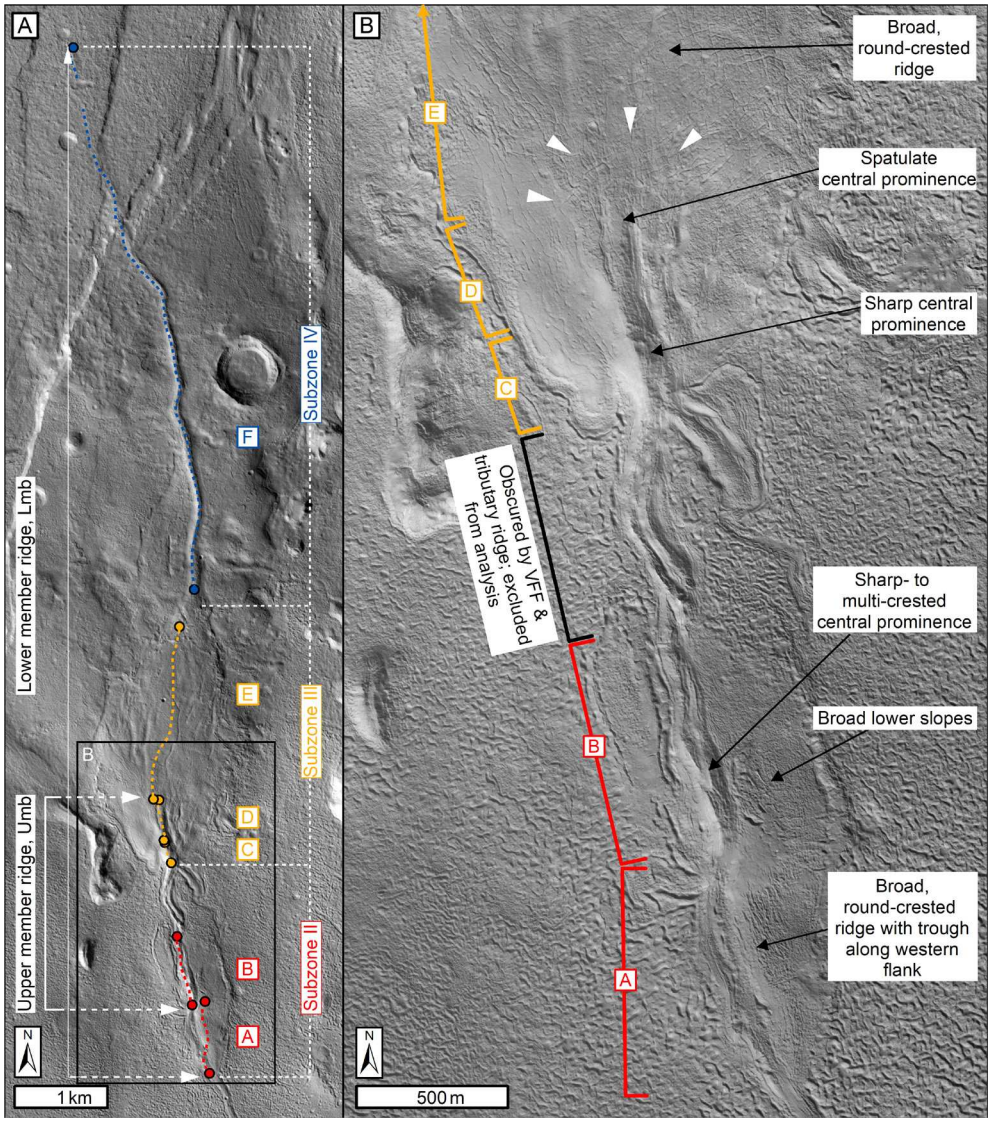

Fig. 4. Morphometric domains of the NW Tempe Terra esker in context. (A) CTX image mosaic showing extents of morphometric domains (points joined by coloured dotted lines), relative to morphological subzones defined by Butcher et al. (2017) and the upper and lower member ridges (white arrowed brackets). The black box shows the extent of (B), an orthorectified HiRISE image of domains A–D, and the southern portion of domain E. White arrows indicate the location where the spatulate portion of the Umb becomes topographically indistinct (i.e. the Umb terminus). See Appendix A for data products. Colours in all panels represent subzones defined by Butcher et al. (2017).

to domain F. Domain F has a narrow, sharp-crested morphology (Fig. 4; Fig. 5I). Like domain E, domain F exhibits no distinct central prominence. Visually, the domain F ridge is similar in width to both the central prominence in domains B and C (Fig. 5D and F), and to the inter-crest trough in domain B (Fig. 5B).

4.3. The stacked esker hypothesis

The observations described above lead us to propose that domains A–D of the NW Tempe Terra esker form a 'stacked' esker *formation* comprising two morphologically-distinct esker ridges (which we term *members*) which formed under a multi-stage esker deposition regime. We hypothesise that the raw heights measured for domains B–D (Fig. 3) represent the composite heights of these stacked ridge members: (1) a broad underlying ridge in domains B–D which is continuous with domains E and F, and we term the *lower member* (Lmb) ridge; and (2) a narrower secondary ridge (the *upper member*, Umb) that was deposited atop the Lmb in domains B–D. Following this hypothesis, we propose that domain A was originally round-crested, and that the inter-crest trough part way down its gently-sloping western flank was eroded by meltwater supplying the Umb in domains B–D.

4.4. Tests of the stacked esker hypothesis

4.4.1. Approach

To explore the stacked esker hypothesis, we first made predictions about the height-width trends that would be observed if the signals of the Umb and Lmb ridges were separated. The Lmb comprises two domains where there is no evidence for a superposed ridge (domains E and F); domain E has a simple, broad, round-crested morphology, while domain F has a simple, narrow, sharp-crested morphology. We used the morphometries of these domains as 'reference morphometries', upon which we based our predictions of the height-width trends of morphologically-similar portions of the constituent Umb and Lmb ridges in the stacked domains (Fig. 6A). Observations of eskers on Earth suggest that the crest morphologies and geometries of eskers could be related to the dynamics of their formation (e.g., Burke et al., 2015). Our predictions assume that esker morphometry is process-controlled, and therefore that portions of martian eskers with similar crest mor-

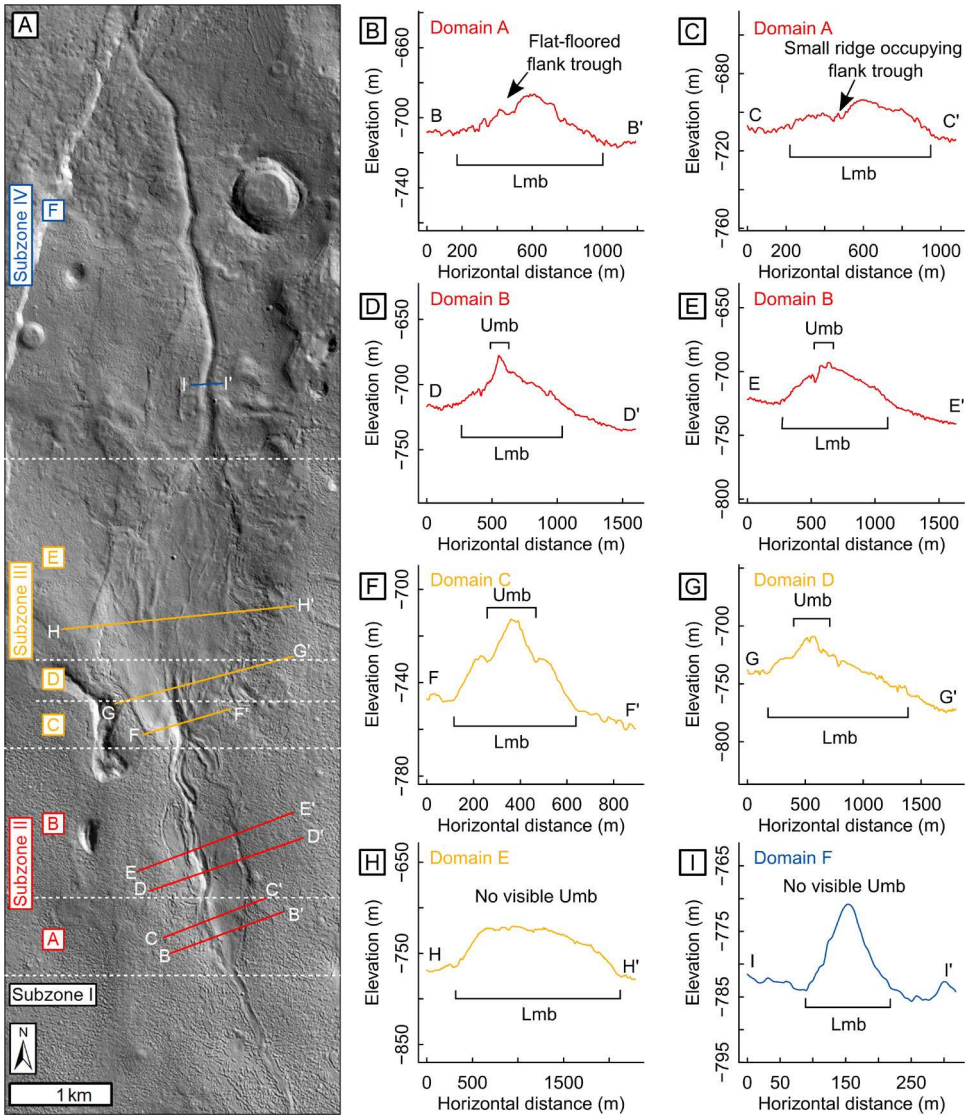

Fig. 5. Domains of the NW Tempe Terra esker in topographic profile. (A) CTX image mosaic showing locations (solid lines) of HiRISE cross-sectional topographic profiles in subsequent panels. White dotted lines indicate subzone and domain transitions. Colours in all panels represent subzones defined by Butcher et al. (2017). Panels B–I are topographic profiles: (B) B–B' showing the wide, round-crested ridge in domain A with a flat-floored trough in its western flank; (C) C–C' showing the wide, round-crested ridge in domain A, at the location where the upper member ridge appears to originate as a proto-ridge occupying a trough on the western flank; (D) D–D' showing a sharp-crested portion of the upper member (Umb) in domain B, atop the wider, round-crested lower member ridge (Lmb); (E) E–E' showing a multi-crested portion of the upper member in domain B, atop the wider, round-crested Lmb; (F) F–F' showing the wide lower member ridge superposed by a prominent sharp-crested portion of the upper member in domain C; (G) G–G' showing the wide lower member ridge superposed by the low, spatulate terminus of the upper member ridge in domain D; (H) Profile H–H' showing the wide, round-crested morphology of domain E, which lacks a visible upper member ridge; (I) Profile I–I', showing the sharp-crested morphology in domain F, which lacks a visible upper member ridge. All topographic profiles are at 10 × vertical exaggeration.

phologies, scales, and degradation states formed by similar processes, and have similar height-width relationships.

Under the stacked esker hypothesis, the flat-floored inter-crest trough in domain A formed by erosion into the surface of the Lmb by meltwater supplying the Umb down-conduit. Since this hypothesised secondary erosion occurred along the flank of the Lmb, we suggest that the height of the central crest of the ridge in domain A is representative of the original height of the Lmb in this domain, which would have been round-crested prior to flank trough incision. This is supported by the similarity in raw height-width trend between domain A and the round-crested portion of the Lmb in domain E. Thus, we use transects in domains A and E for reference morphometries of round-crested ridge portions.

To test our predictions, we extracted height and width measurements for the Umb in domains B–D, using the same method and transects as for the raw measurements, with the key difference that we classified the base points of the inferred Umb rather than the full ridge formation. We subtracted the Umb heights from the raw height measurements to approximate the Lmb height, then replotted the height-width scatterplot with the Umb and Lmb separated (Fig. 6B) to test whether they followed the predicted trends (Fig. 6A). The uncertainty in height measurements of the constituent Umb and Lmb ridges is compounded by subtraction of the Umb height from the raw height. We calculated this uncertainty as ±3 m (see Appendix C). The uncertainty in width remains the same as that for the raw width measurements (Section 3.4).

4.4.2. Predictions

If the stacked esker hypothesis is correct, subtracting the height of the Umb from the total height of the ridge formation in domains B–D should return similar Lmb height-width trends to the reference trends described by the Lmb in domains A and E (Fig. 6A), where the ridge has a similar broad morphology but with no evidence of a superposing ridge.

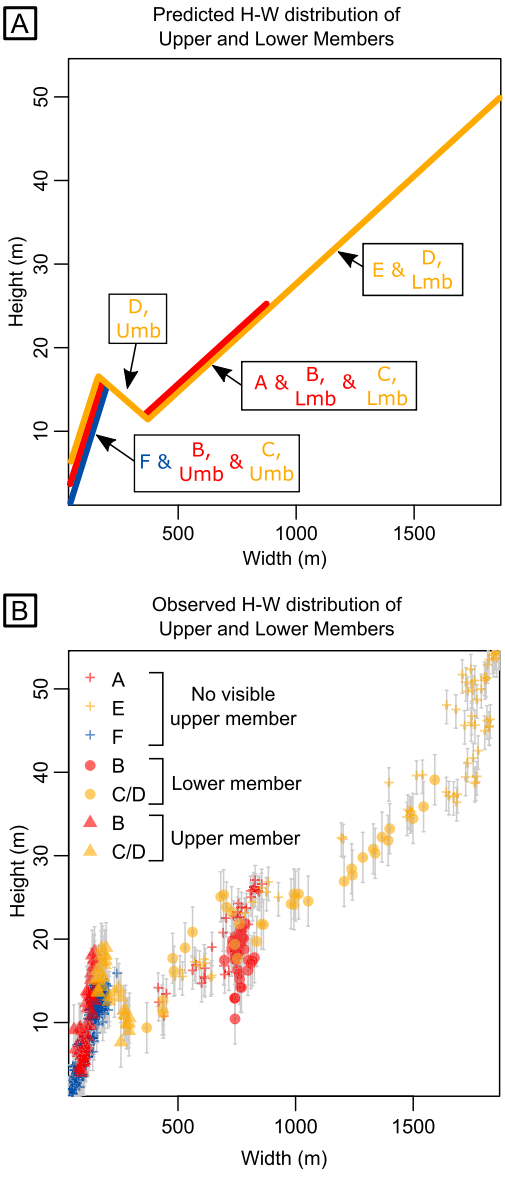

Fig. 6. Predicted and observed height-width relationships for the upper and lower member ridges of the NW Tempe Terra esker formation. (A) Schematic showing predicted trends of height and width measurements of the upper and lower member ridges of the NW Tempe Terra esker formation. Predictions are based on trends for domains with similar crest morphologies, but no visible upper member ridge (Fig. 3B). Labels indicate predicted positions of constituent ridge members and domains in the scatterplot. (B) Actual distribution of upper (triangles) and lower (points) members of the ridge relative to domains where there is no visible upper member ridge (crosses). Colours in both panels represent subzones as defined by Butcher et al. (2017).

The approximate visual similarity between the sharp- to multi-crested Umb in domains B–C (Fig. 4 and Fig. 5D–F), and the simple, sharp-crested portion of the Lmb in domain F (Fig. 5A and I), also leads us to predict that measurements of the Umb in domains B–C would follow a similar height-width trend to the Lmb in domain F (Fig. 6A). We note, however, that the Lmb in domain F is entirely sharp-crested, whereas the Umb in domains B–C has multi-crested sections for which there is no direct analogue in the unstacked portions of the esker formation. Hence, while we expect to observe a broadly similar height-width relationship for the sharp- to multi-crested portions of the Umb, we expect some deviation from the reference trend.

Finally, since the spatulate terminus of the Umb in domain D extends from the tallest part of the Umb in domain C, and lowers and widens northward, grading into the broader lower-member ridge in domain E, we predict that its height-width relationship will follow a negative trend connecting the upper height-width range of domain F to the lower height-width range of domain A points in the height-width scatterplot (Fig. 6A).

If all of the above predictions are correct, the complex groupings of the raw height-width scatterplot in Fig. 3A should effectively collapse onto the reference trends described by the portions of the Lmb with no evidence for a superposed ridge (domains A, E, and F), as illustrated in Fig. 6A.

4.4.3. Observations

The scatterplot in Fig. 6B illustrates that, as predicted, the morphometries of the constituent upper and lower members of the ridge in domains B–C collapse onto the existing reference trends described by portions of the ridge with similar crest morphologies where there is no distinct central prominence (domains A, E, and F; Fig. 3B). Also consistent with our predictions, the spatulate terminus of the Umb in domain D follows a transitional negative trend between the upper range of domain F dimensions and the lower range of domain A dimensions. The small number of points in domain B (Lmb) that appear to have heights ∼2–5 m below the general trend for the Lmb (Fig. 6B) represent locations where the Umb sits within a ∼2–5 m deep trough in the surface of the Lmb. Therefore, the relatively low heights of these points can be explained by underestimation of the true Lmb height resulting from subtraction of the Umb height from the full height of the formation.

Thus, visually, our measurements support our hypothesis that the NW Tempe Terra esker is a stacked esker formation comprising a wide, round-crested lower member ridge in domains A–E which transitions into a sharp-crested ridge in domain F, and a narrower, sharp- to multi-crested upper member ridge which superposes the lower member ridge in domains B–D.

Statistical analyses, which we describe in Appendix E, also support our hypothesis. To summarise, we find no statistically significant difference between the reference and observed trends for the Lmb in domains B–D. While we do identify small but statistically significant differences between the reference and observed trends for the Umb in domains B and C, such differences were expected (Section 4.4.2) owing to slight differences in crest morphology between these ridge portions and the Lmb in domain F, on which the predicted trend was based. Thus, the small differences between the predicted and observed trends do not pose a significant challenge to our hypothesis.

4.5. 3D morphometries of the constituent domains and members of the stacked esker formation

The modified 3D morphometry distributions for the constituent upper and lower members of the NW Tempe Terra esker, categorised by crest morphology, are displayed in Fig. 7.

Descriptive statistics are displayed in Appendix F. These measurements include width-height ratios. We calculated the uncertainty in width-height ratios to be ±6 (Appendix C).

5. Discussion

5.1. Sediment-discharge dynamics of esker formation

Eskers on Earth are widely used for reconstructing the evolution of glaciers and ice sheets, and their drainage systems (e.g., Kleman et al., 1997; Boulton et al., 2001; Storrar et al., 2014b; Burke et al., 2015; Stroeven et al., 2016). Where there has been limited post-depositional modification, esker morphology and sedimentology provide insights into the temporal evolution of drainage

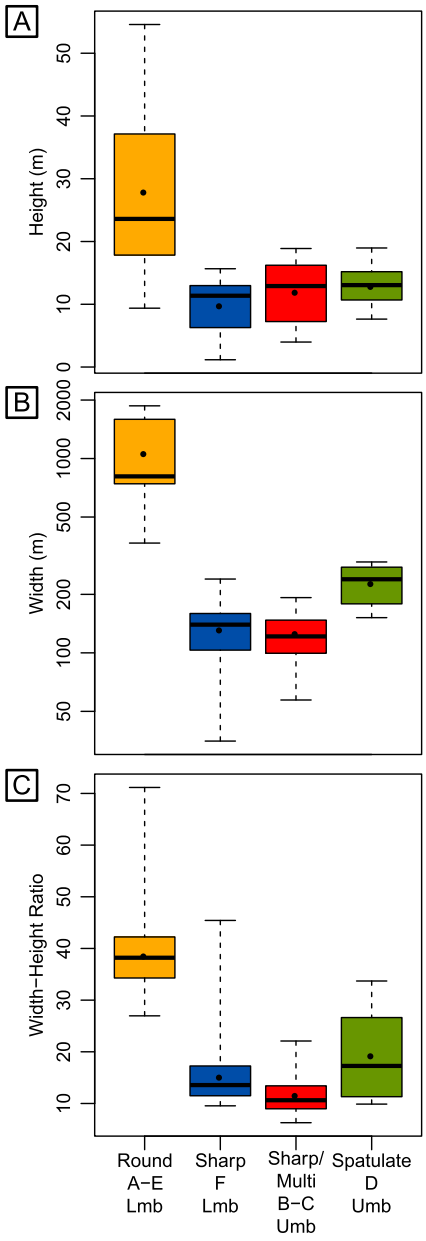

Fig. 7. Boxplots showing (A) heights, (B) widths, and (C) width-height ratios of the upper and lower member ridges of the NW Tempe Terra esker formation, categorised by domain and crest morphology. Note logarithmic scale on width plot. In all boxplots, boxes represent the interquartile range, dashed whiskers represent maximum and minimum, solid bars represent the medians, and points represent the means.

dynamics under changing meltwater and sediment supply regimes (e.g., Shreve, 1985; Burke et al., 2008, 2010; Storrar et al., 2014b; Burke et al., 2012; Perkins et al., 2013; Burke et al., 2015). Reconstructions of the dynamics of esker-forming melt events on Earth can be achieved via field studies of the structure and properties of esker interior sediments (e.g., Banerjee and McDonald, 1975; Brennand, 1994, 2000; Burke et al., 2008, 2010; Cummings et al., 2011; Burke et al., 2012; Perkins et al., 2013; Burke et al., 2015; Perkins et al., 2016). Recent studies have identified relationships between the interior sedimentology and macro-scale morphology of eskers on Earth (e.g., Burke et al., 2015; Perkins et al., 2016).

Candidate eskers on Mars are currently inaccessible except by orbital remote sensing. However, terrestrial insights can aid understanding of the dynamics of esker-forming drainage events on Mars, where metre-scale morphometric observations are enabled by high-resolution remote sensing datasets, but sub-metre-scale sedimentary observations are not currently possible. Based on terrestrial insights, we propose that the stacked morphology of the NW Tempe Terra esker reflects at least two stages of esker deposition within the esker-forming subglacial meltwater conduit, either during the same meltwater drainage episode, or during two or more distinct drainage episodes.

In their qualitative analyses, Butcher et al. (2017) suggested that the subzone-scale transitions in crest morphology along the esker are consistent with the progression of esker morphology that Shreve (1985) predicted as an esker-forming meltwater conduit approaches, ascends, and then descends an undulation in the bed. However, field studies (Banerjee and McDonald, 1975; Brennand, 1994; Burke et al., 2008, 2010, 2012, 2015; Perkins et al., 2016) have shown that esker morphology is also intimately linked to sediment-discharge dynamics that complicate conduit evolution and esker sedimentation beyond Shreve's model (Shreve, 1985).

Given the new morphometric insights presented here, we modify our earlier hypothesis (Butcher et al., 2017) and argue that dynamic sediment-discharge processes could provide a better explanation for the transitions in crest morphology, both along the landform and between its lower and upper members. What follows is a summary of the relevant theory pertaining to sediment-discharge controls on terrestrial esker morphology, which we then assimilate into first-order conceptual models for the spatiotemporal variations in sediment-discharge regime that could explain our new morphometric observations.

5.1.1. Sediment-discharge dynamics and the morphology of eskers on Earth

On Earth, ridge enlargements along eskers, akin to the broad, tall, round-crested Lmb in domains A–E of the NW Tempe Terra esker, commonly comprise large, architecturally complex sedimentary depocentres (macroforms) recording upflow, downflow, vertical, and lateral accretion (e.g., Brennand, 1994, 2000; Burke et al., 2008, 2010, 2012, 2015; Perkins et al., 2016).

As illustrated in Fig. 8 (column a), deposition of bedforms on the conduit floor can obstruct the flow of conduit-confined meltwater under conditions of high sediment supply and flow power (e.g., Brennand, 1994; Burke et al., 2008, 2010, 2012, 2015). Resultant focussing of meltwater flow increases hydraulic pressure and flow power, promoting vertical, lateral, and/or longitudinal expansion of the conduit by wall and roof melting (e.g., Brennand, 1994; Burke et al., 2008, 2010, 2012, 2015). Cavities formed on the stoss and/or lee sides of a bedform due to conduit enlargement drive a reduction in flow power, encouraging further macroform growth by upflow, downflow, lateral, and/or vertical aggradation. This forms a positive feedback of conduit migration and macroform growth (Brennand, 1994; Burke et al., 2015), and results in formation of laterally- and vertically-enlarged ridge morphologies (e.g., Burke et al., 2015).

In contrast, narrow, sharp- to round-crested portions of eskers typically lack the complex ridge morphologies associated with macroforms. They typically have relatively simple sedimentary architectures comprising tabular or arched beds (e.g., Brennand, 1994, 2000; Burke et al., 2012, 2008, 2010, 2015). This contrast has been attributed to differences in sediment supply and flow power during formation of narrow portions of eskers and macroform-dominated ridge enlargements. Under moderate sediment supply scenarios, deposition along the conduit is more uniform, allowing deposition of quasi-continuous tabular beds (Fig. 8, column b) and uniform conduit growth that is dominated by vertical roof melting (Banerjee and McDonald, 1975; Brennand, 2000; Burke et al., 2015). This results in formation of narrow sharp- and round-crested eskers. If sediment supply is strongly limited, conduit growth is controlled almost exclusively by meltwater dis-

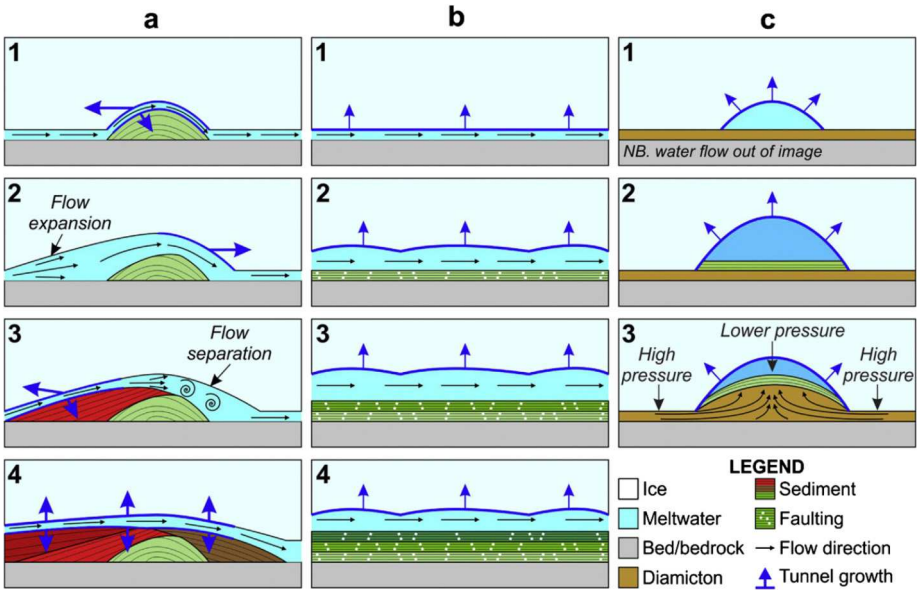

Fig. 8. Schematic showing the theoretical evolution of an esker-forming drainage conduit under different sediment supply and flow power regimes. Columns a–c are different sediment supply and flow power scenarios, and rows 1–4 show temporal evolution of the conduit under those scenarios. Column a shows depocentre growth under high sediment supply and high flow power conditions. Column b shows a limited sediment supply and high flow power scenario. Column c shows a flow-transverse cross-section of the conduit, under limited sediment supply conditions, accompanied by a drop in meltwater discharge (row 3). See text for explanation. Not to scale. Reproduced from Burke et al. (2015).

charge, and sedimentation in the conduit is low or absent. If a discharge reduction occurs more rapidly than the conduit can shrink to compensate for the associated reduction in hydraulic pressure, steep pressure gradients between the bed and the conduit can encourage deformation of bed sediments into the conduit, forming arched beds, often with a core of diamicton (Fig. 8, column c; Burke et al., 2015).

By extension, transitions from complex up-conduit ridge enlargements to relatively simple, narrow, sharp- or round-crested esker morphologies have been attributed to down-conduit reductions in sediment supply associated with macroform growth at those ridge enlargements (Brennand, 1994; Burke et al., 2015).

Multi-crested eskers on Earth, similar to the multi-crested portion of the Umb in domains A–B of the NW Tempe Terra esker, have been attributed to exploitation of structural weaknesses (e.g., fractures) and/or flow divergence around ice blocks under high flow power conditions (Burke et al., 2012; Perkins et al., 2016), or formation of eskers in englacial conduits and subsequent let-down and loss of an internal ice core (Price, 1966).

5.2. Multi-stage dynamics of esker formation in NW Tempe Terra, Mars

Fig. 9 illustrates two possible conceptual models that could explain the stacked morphology of the NW Tempe Terra esker formation, and morphological transitions along the landform. These scenarios are by no means exhaustive; we restrict the scope of this study to simple 'single-pipe' scenarios, which assume that synchronous sedimentation was possible along the entire length of a conduit of similar length to the present-day landform. We discuss this assumption further in Section 5.3.

Under both models, Lmb formation dynamics (Section 5.2.1) are the same. The models diverge in their temporal placement of Umb formation (Section 5.2.2). Considering our sampling strategy (Section 3.3), we do not speculate on the dynamics of esker formation upflow of domain A.

5.2.1. Formation of the lower member ridge

We propose that the Lmb formed under high discharge and high sediment-supply conditions. Rapid, non-uniform deposition along the conduit became focussed at two depocentres: one located in domains A–B, and one in domains C–E. Vertical, lateral, and longitudinal migration of the conduit around these depocentres (see Section 5.1.1) encouraged cavity formation, which reduced flow power and promoted further deposition, initiating a positive feedback of depocentre and conduit growth, and explaining the enlarged morphologies in domains A–B and C–E. The tapered margins and gradual lowering of the broad, round-crested portion of the ridge towards the domain E–F transition (Fig. 4A) are consistent with streamlining of esker sediments, and possibly the conduit itself in the lee cavity of a sedimentary depocentre in domains C–E (Fig. 9; Burke et al., 2015).

Beyond the tapered domain E–F transition, the conduit adopted a relatively narrow geometry. Depocentre growth in domains A–E restricted sediment supply down-conduit, permitting more uniform growth of the conduit in domain F. Thus, here, the resulting esker deposit was narrow (Fig. 9) and sharp-crested. There is no evidence for deformation of the bed adjacent to the ridge in domain F, so we suggest that the esker accumulated via gradual accretion under moderate sediment supply conditions, rather than pressure-driven deformation of surrounding bed materials under a sediment-starved regime (see Section 5.1).

5.2.2. Formation of the upper member ridge

Following the sediment-discharge model of Burke et al. (2015), we suggest that the sharp- to multi-crested Umb formed within a narrow conduit that passed along the flank and crest of the Lmb in domains A–D. We propose two possible conceptual models (A and B) for the formation of the upper member ridge. These models differ in their temporal placement of Umb formation. In model A (Fig. 9, panels 1–3), the Umb formed under a changing sediment-discharge regime during the same drainage episode as the Lmb. In model B (Fig. 9, panels 4–6), the Umb formed during a second, distinct drainage episode, following significant (~6 km) retreat of the glacier terminus across domain F of the Lmb. Before describ-

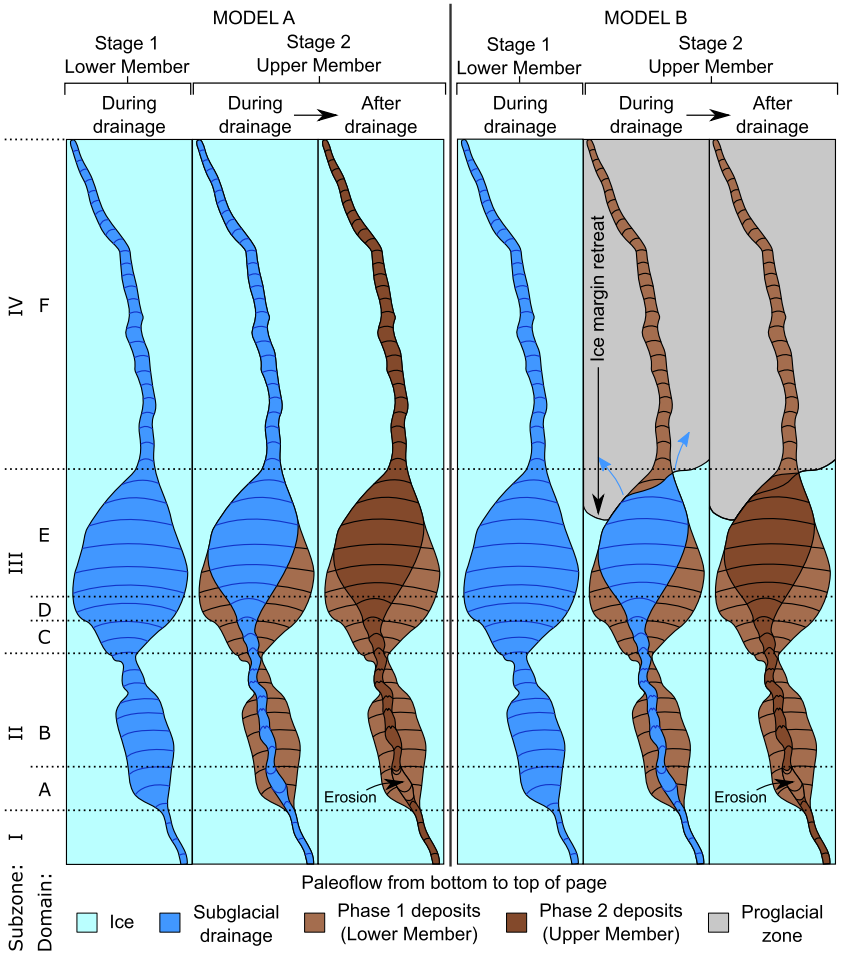

Fig. 9. Schematic showing two possible models for the formation of the stacked esker morphology in NW Tempe Terra, Mars. The conduit is located at the glacier bed and is confined at its roof and walls by glacial ice. Meltwater flow is towards the top of the panels, and ice thickness reduces towards the top. Black dotted lines show transitions between morphological subzones as defined by Butcher et al. (2017), and morphometric domains defined in the present study. Models A and B diverge in their temporal placement of Umb formation. In model A (panels 1–3), the Umb formed during a second stage of flow within the same drainage episode during which the Lmb was deposited. Model B (panels 4–6) places Umb formation during a distinct melt episode, following retreat of the ice terminus to the location of the esker-transverse moraine-like ridge identified by Butcher et al. (2017). We do not speculate on the dynamics of ridge formation to the south since this is largely obscured by remnant VFF materials. See text for full description of model.

ing these models, we first discuss some pertinent morphological aspects of the ridge that may provide insight on Umb formation.

In Section 4.3, we interpreted the inter-crest trough on the flank of the Lmb in domain A as a meltwater-incised trough based on its flat-floored morphology (Fig. 5B), and its alignment and similarity in width with the Umb. The trough crosses a topographic high along the Lmb, which is consistent with Shreve's (1985) prediction that topographic undulations in the bed (in this case, the upper surface of the Lmb) focus lines of hydraulic equipotential at their peaks, locally increasing flow power such that non-deposition, or even erosion, can occur. The proto-ridge infilling the northernmost portion of the flank trough in domain A could therefore mark the location where erosion transitioned to deposition on the lee slope of the peak.

Unlike the sharp-crested portion of the Lmb in domain F, portions of the Umb are located within a shallow (~2–5 m deep) trough (e.g., Fig. 5F). Thus, it is plausible that the parent meltwater conduit was strongly sediment starved, and the Umb primarily comprises sediment scavenged from the Lmb following a sudden reduction in hydraulic pressure (see Section 5.1). However, it is also possible that this trough represents a period of erosive flow prior to the onset of Umb deposition under a moderate sediment supply regime. A mass-balance approach comparing Umb volume with the volume of the trough could aid discrimination between these scenarios. However, given the unavoidable lack of sedimentary observations to supplement such analyses, we do not speculate further on which regime prevailed.

We suggest that the multi-crested portion of the Umb represents a location where high flow power forced meltwater into structural weaknesses in the conduit roof. The location of the multi-crested portion of the ridge within a shallow trough in the Lmb provides strong evidence for direct interaction of meltwater with the surface of the Lmb. This is inconsistent with the alternative mechanism by which multi-crested eskers can form on Earth, i.e. by loss of an internal ice core following esker let-down from an englacial or supraglacial position (Price, 1966).

5.2.2.1. Model A: formation of Umb during the late stages of a single drainage episode In model A, we propose that the Umb was deposited atop the Lmb as sediment supply and/or meltwater discharge waned towards the end of the same drainage episode that formed the Lmb. In domains A–C, the conduit shrank to equilibrate hydraulic pressure with ice overburden pressure, and flow became focused along the relatively narrow path of the Umb (Fig. 9, panel 2). Conduit shrinkage maintained hydraulic pressure, allowing meltwater to ascend the flanks of the Lmb and pass along its crest.

As the conduit approached thinner ice towards the glacier terminus, the tendency for conduit closure under waning discharge reduced and the conduit retained its earlier geometry northward of domain D (Fig. 9, panel 2). As meltwater passed into the broader conduit across the domain C–D transition, its flow power reduced and sediment dispersed over the surface of the Lmb, forming the spatulate Umb terminus in domain D. Sedimentation probably continued northward of the spatulate deposit (Fig. 9, panel 3), but a reduced tendency for conduit closure beneath thin ice approaching the glacier terminus meant that late-stage sedimentation was indistinct from the earlier stage(s), and there was no notable vertical transition in the morphology of the resulting ridge crest.

5.2.2.2. Model B: formation of Umb during a temporally-distinct drainage episode Model B provides an alternative explanation for the lack of a morphologically-distinct Umb northward of the domain D–E transition. It places Umb formation during a temporally-distinct drainage episode, following retreat of the glacier terminus towards the spatulate terminus of the Umb (Fig. 9, panel 5), possibly to the transverse ridge that crosses the esker crest at the domain E–F transition. Butcher et al. (2017) interpreted this transverse ridge as a recessional moraine. We do not speculate on the period over which terminus retreat may have occurred. A second drainage episode re-established a meltwater pathway over the unexposed portion of the Lmb, either because the earlier conduit did not shut down completely, or because the pre-existing topography of the Lmb induced hydraulic gradients towards thinner ice at its crest. Sediment supply and/or meltwater discharge were lower during the second drainage episode, allowing development of a narrow conduit atop the Lmb (Fig. 9, panel 5). Proximal to the ice margin, subglacial meltwater conduits commonly expand into larger portals. The spatulate terminus of the Umb in domain D could represent dispersal of flow as the conduit entered a terminal portal.

5.3. Spatiotemporal nature of esker deposition in NW Tempe Terra

The up-glacier extent over which esker deposition is possible, and the timescales of esker deposition relative to ice-margin retreat rates on Earth are topics of ongoing debate (Shreve, 1985; Brennand, 1994, 2000; Hooke and Fastook, 2007; Burke et al., 2008, 2010; Cummings et al., 2011; Storrar et al., 2014a). Some workers theorise that eskers can form synchronously within continuous, steady-state drainage conduits extending over the full length of the resulting esker, for example during short-duration, high-magnitude outburst floods (e.g., Burke et al., 2008, 2010; Storrar et al., 2015). Others suggest that time-transgressive, headward aggradation behind a retreating ice margin over interannual timescales better explains esker formation (e.g., Banerjee and McDonald, 1975; Aylsworth and Shilts, 1989; Clark and Walder, 1994; Hooke and Fastook, 2007; Cummings et al., 2011; Storrar et al., 2014b, 2014a). In reality, both mechanisms have probably prevailed in different locations on Earth, but it is not known which mechanism is the most common.

Our observations of the NW Tempe Terra esker provide ambiguous evidence for the spatiotemporal nature of esker deposition. The models presented here are single-pipe models and inherently assume that synchronous deposition was possible along the full length of the landform during one or more drainage episodes. More complex scenarios whereby sedimentation was focussed close to a retreating ice margin are beyond the scope of this study but are an important topic for future research. However, the current inaccessibility of the landform for detailed sedimentary studies would restrict the ability to test such models. Nonetheless, the lack of depositional fan at the northernmost terminus of the Lmb is most consistent with synchronous formation under short-timescale, high-magnitude drainage (Burke et al., 2012). It is possible that the Lmb in domains C–E is such a fan deposit, but its tapered morphology towards the domain E–F transition is more consistent with streamlining of esker sediments in the lee cavity of a subglacial depocentre. Evidence for ascent of bedslopes and possibly exploitation of structural weaknesses in the conduit roof during formation of the sharp- to multi-crested Umb provides evidence for rapid-onset, high flow-power drainage (e.g., Burke et al., 2010, 2012; Perkins et al., 2016).

Model B, which invokes two distinct stages of esker aggradation at a retreating ice margin is inherently time-transgressive. However, the individual ridge members could effectively have formed synchronously during their respective aggradation stages. Unless drainage was quasi-continuous throughout glacier retreat, model B requires at least two distinct drainage episodes.

Formation of the NW Tempe Terra esker during a single, multi-stage drainage episode (model A) is more consistent than model B with the hypothesis that late-Amazonian esker forming melt events were driven by transient geothermal heating of the basal ice (Gallagher and Balme, 2015; Butcher et al., 2017). The occurrence of two distinct geothermal events under model B seems less likely than a single event under model A, but cannot be ruled out.

5.4. Implications for sediment production in NW Tempe Terra

Formation of the esker during a transient melt episode that punctuated a long-term cold-based thermal regime (Butcher et al., 2017) could be problematic for the high sediment-supply regime invoked to explain morphological transitions along the Lmb (Section 5.2.1). Typically, cold-based glaciers are associated with extremely low rates of sliding and erosion at their beds, although erosion may be more significant when integrated over long timescales (e.g., Shreve, 1984; Echelmeyer and Wang, 1987; Cuffey et al., 2000). However, weakened bedrock supplies abundant sediment to the surfaces and beds of glaciers in high-relief, tectonic settings on Earth (Hallet et al., 1996). Therefore, the steep-sided scarps that bound the tectonic rift valley hosting the NW Tempe Terra esker could have provided sediment to the glacier bed. Flow convergence of glacial ice at the base of the rift-bounding fault scarps (Butcher et al., 2017) could have induced high basal stress gradients relative to VFFs in non-convergent settings, further encouraging mechanical erosion of weakened bedrock. Additionally, VFFs on Mars could comprise ~10% debris by volume (e.g., Holt et al., 2008). Thus some sediment could have been supplied to the esker by melt-out of debris from the conduit roof and/or walls.

6. Conclusions

We characterise the metre-scale morphometry of the late-Amazonian-aged glacier-linked esker identified by Butcher et al. (2017) in NW Tempe Terra, Mars. We use these morphometries to reconstruct the possible multi-stage dynamics (including spatiotemporal variations in sediment and discharge) of esker formation. We find that the NW Tempe Terra esker comprises two stacked esker ridges which probably record spatial and temporal evolution of the parent subglacial drainage conduit in response to variations in sediment supply and/or meltwater discharge. Spatial variations in sediment supply due to growth of sedimentary depocentres (and resulting limitation of sediment supply down conduit) could explain the transition from an enlarged, round-crested morphology to a narrow, sharp-crested morphology along the underlying lower member ridge. A temporal reduction in discharge and/or sediment supply, either during or between the esker-forming drainage episode(s), could explain the superposition of the narrow, sharp- to multi-crested upper member ridge atop the

broad portions of the lower member ridge. We explore the stacked esker hypothesis using a novel morphometric approach which uses observed morphometric reference relationships to predict the height-width trends for portions of the ridge with similar crest morphologies. We observe close similarities between predicted and observed trends, suggesting that the height-width relationships of eskers on Mars with similar crest morphologies and degradation states could be predictable. If confirmed by our ongoing morphometric comparisons with other candidate eskers on Mars and on Earth, the observed relationships could be used more widely as reference relationships against which sinuous ridges elsewhere on Mars (e.g., Gallagher and Balme, 2015) can be compared during tests for esker origins of those ridges. The systematic quantification of esker morphometry presented here will also provide constraints for future numerical modelling experiments aiming to constrain the nature of conduit evolution and esker sedimentation on Mars, and the environmental and glaciological drivers of esker-forming meltwater generation.

Declaration of competing interest

The authors declare that they have no known competing financial interests or personal relationships that could have appeared to influence the work reported in this paper.

Acknowledgements

We thank two anonymous reviewers, whose suggestions helped us to improve the clarity of the manuscript. This work was undertaken at The Open University as part of a PhD studentship held by FEGB and funded by the Science Technology and Facilities Council (STFC) grant ST/N50421X/1. Manuscript preparation was supported by The Open University (internal funding) and the European Research Council (ERC) under the European Union's Horizon 2020 research and innovation programme (ERC Advanced Grant PALGLAC 787263). We also gratefully acknowledge UK Space Agency grants ST/L00643X/1, ST/R001413/1, and ST/R001383/1 (MRB); ST/R001405/1, ST/P001262/1, and ST/S00145X/1 (SRL); and ST/R/001375 (AH). SJC is supported by the French space agency, CNES.

Appendix. Supplementary material

Supplementary material related to this article can be found online at https://doi.org/10.1016/j.epsl.2020.116325.

References

Arnold, N.S., Conway, S.J., Butcher, F.E.G., Balme, M.R., 2019. Modeled subglacial water flow routing supports localized intrusive heating as a possible cause of basal melting of Mars' South polar ice cap. J. Geophys. Res., Planets 124, 2101–2116. https://doi.org/10.1029/2019JE006061.

Aylsworth, J.M., Shilts, W.W., 1989. Bedforms of the Keewatin ice sheet, Canada. Sediment. Geol. 62, 407–428. https://doi.org/10.1016/0037-0738(89)90129-2.

Banerjee, I., McDonald, B.C., 1975. Nature of esker sedimentation. In: Jopling, A.V., McDonald, B.C. (Eds.), Glaciofluvial and Glaciolacustrine Sedimentation: Society of Economic Paleontologists and Mineralogists, Special Publication, pp. 304–320.

Boulton, G.S., Dongelmans, P., Punkari, M., Broadgate, M., 2001. Palaeoglaciology of an ice sheet through a glacial cycle: the European ice sheet through the Weichselian. Quat. Sci. Rev. 20, 591–625. https://doi.org/10.1016/S0277-3791(00)00160-8.

Brennand, T.A., 1994. Macroforms, large bedforms and rhythmic sedimentary sequences in subglacial eskers, South-central Ontario: implications for esker genesis and meltwater regime. Sediment. Geol. 91, 9–55. https://doi.org/10.1016/0037-0738(94)90122-8.

Brennand, T.A., 2000. Deglacial meltwater drainage and glaciodynamics: inferences from Laurentide eskers, Canada. Geomorphology 32, 263–293. https://doi.org/10.1016/S0169-555X(99)00100-2.

Burke, M.J., Brennand, T.A., Perkins, A.J., 2012. Transient subglacial hydrology of a thin ice sheet: insights from the Chasm esker, British Columbia, Canada. Quat. Sci. Rev. 58, 30–55. https://doi.org/10.1016/j.quascirev.2012.09.004.

Burke, M.J., Brennand, T.A., Sjogren, D.B., 2015. The role of sediment supply in esker formation and ice tunnel evolution. Quat. Sci. Rev. 115, 50–77. https://doi.org/10.1016/j.quascirev.2015.02.017.

Burke, M.J., Woodward, J., Russell, A.J., Fleisher, P.J., Bailey, P.K., 2008. Controls on the sedimentary architecture of a single event englacial esker: Skeiðarárjökull, Iceland. Quat. Sci. Rev. 27, 1829–1847. https://doi.org/10.1016/j.quascirev.2008.06.012.

Burke, M.J., Woodward, J., Russell, A.J., Fleisher, P.J., Bailey, P.K., 2010. The sedimentary architecture of outburst flood eskers: a comparison of ground-penetrating radar data from Bering glacier, Alaska and Skeiðarárjökull, Iceland. Geol. Soc. Am. Bull. 122, 1637–1645. https://doi.org/10.1130/B30008.1.

Butcher, F.E.G., Balme, M.R., Gallagher, C., Arnold, N.S., Conway, S.J., Hagermann, A., Lewis, S.R., 2017. Recent basal melting of a mid-latitude glacier on Mars. J. Geophys. Res., Planets 122, 2445–2468. https://doi.org/10.1002/2017JE005434.

Butcher, F.E.G., Conway, S.J., Arnold, N.S., 2016. Are the Dorsa Argentea on Mars eskers? Icarus 275, 65–84. https://doi.org/10.1016/j.icarus.2016.03.028.

Clark, P.U., Walder, J.S., 1994. Subglacial drainage, eskers, and deforming beds beneath the Laurentide and Eurasian ice sheets. Geol. Soc. Am. Bull. 106, 304–314. https://doi.org/10.1130/0016-7606(1994)106<0304:SDEADB>2.3.CO;2.

Cuffey, K.M., Conway, H., Gades, A.M., Hallet, B., Lorrain, R., Severinghaus, J.P., Steig, E.J., Vaughn, B., White, J.W.C., 2000. Entrainment at cold glacier beds. Geology 28, 351–354. https://doi.org/10.1130/0091-7613(2000)28<351:EACGB>2.0.CO;2.

Cummings, D.I., Gorrell, G., Guilbault, J.-P., Hunter, J.A., Logan, C., Ponomarenko, D., André, J.-M.P., Pullan, S.E., Russell, H.A.J., Sharpe, D.R., 2011. Sequence stratigraphy of a glaciated basin fill, with a focus on esker sedimentation. Geol. Soc. Am. Bull. 123, 1478–1496. https://doi.org/10.1130/B30273.1.

Echelmeyer, K., Wang, Z., 1987. Direct observation of basal sliding and deformation of basal drift at sub-freezing temperatures. J. Glaciol. 33, 83–98. https://doi.org/10.3189/S0022143000005396.

Gallagher, C., Balme, M., 2015. Eskers in a complete, wet-based glacial system in the Phlegra Montes region, Mars. Earth Planet. Sci. Lett. 431, 96–109. https://doi.org/10.1016/j.epsl.2015.09.023.

Hallet, B., Hunter, L., Bogen, J., 1996. Rates of erosion and sediment evacuation by glaciers: a review of field data and their implications. Glob. Planet. Change 12, 213–235. https://doi.org/10.1016/0921-8181(95)00021-6.

Holt, J.W., Safaeinili, A., Plaut, J.J., Head, J.W., Phillips, R.J., Seu, R., Kempf, S.D., Choudhary, P., Young, D.A., Putzig, N.E., Biccari, D., Gim, Y., 2008. Radar sounding evidence for buried glaciers in the southern mid-latitudes of Mars. Science 322, 1235–1238. https://doi.org/10.1126/science.1164246.

Hooke, R.L., Fastook, J., 2007. Thermal conditions at the bed of the Laurentide ice sheet in Maine during deglaciation: implications for esker formation. J. Glaciol. 53, 646–658. https://doi.org/10.3189/002214307784409243.

Kleman, J., Hättestrand, C., Borgström, I., Stroeven, A., 1997. Fennoscandian palaeoglaciology reconstructed using a glacial geological inversion model. J. Glaciol. 43, 283–299. https://doi.org/10.3189/S0022143000003233.

McEwen, A.S., Eliason, E.M., Bergstrom, J.W., Bridges, N.T., Hansen, C.J., Delamere, W.A., Grant, J.A., Gulick, V.C., Herkenhoff, K.E., Keszthelyi, L., Kirk, R.L., Mellon, M.T., Squyres, S.W., Thomas, N., Weitz, C.M., 2007. Mars reconnaissance orbiter's high resolution imaging science experiment (HiRISE). J. Geophys. Res. 112, E05S02. https://doi.org/10.1029/2005JE002605.

Perkins, A.J., Brennand, T.A., Burke, M.J., 2013. Genesis of an esker-like ridge over the southern Fraser Plateau, British Columbia: Implications for paleo-ice sheet reconstruction based on geomorphic inversion. Geomorphology 190, 27–39. https://doi.org/10.1016/j.geomorph.2013.02.005.

Perkins, A.J., Brennand, T.A., Burke, M.J., 2016. Towards a morphogenetic classification of eskers: implications for modelling ice sheet hydrology. Quat. Sci. Rev. 134, 19–38. https://doi.org/10.1016/j.quascirev.2015.12.015.

Price, R.J., 1966. Eskers near the Casement glacier, Alaska. Geogr. Ann., Ser. A, Phys. Geogr. 48, 111–125. https://doi.org/10.2307/520521.

R Development Core Team, 2008. R: A Language and Environment for Statistical Computing. R Foundation for Statistical Computing, Vienna, Austria.

Shreve, R.L., 1984. Glacier sliding at subfreezing temperatures. J. Glaciol. 30, 341–347.

Shreve, R.L., 1985. Esker characteristics in terms of glacier physics, Katahdin esker system, Maine. Geol. Soc. Am. Bull. 96, 639–646. https://doi.org/10.1130/0016-7606(1985)96<639:ECITOG>2.0.CO;2.

Sori, M., Bramson, A.M., 2019. Water on Mars, with a grain of salt: local heat anomalies are required for basal melting of ice at the South pole today. Geophys. Res. Lett. 46, 1222–1231.

Squyres, S.W., 1979. The distribution of lobate debris aprons and similar flows on Mars. J. Geophys. Res. 84, 8087–8096. https://doi.org/10.1029/JB084iB14p08087.

Storrar, R.D., Evans, D.J.A., Stokes, C.R., Ewertowski, M., 2015. Controls on the location, morphology and evolution of complex esker systems at decadal timescales, Breiðamerkurjökull, southeast Iceland. Earth Surf. Process. Landf. 40, 1421–1438. https://doi.org/10.1002/esp.3725.

Storrar, R.D., Stokes, C.R., Evans, D.J.A., 2014a. Morphometry and pattern of a large sample (>20,000) of Canadian eskers and implications for subglacial drainage beneath ice sheets. Quat. Sci. Rev. 105, 1–25. https://doi.org/10.1016/j.quascirev.2014.09.013.

Storrar, R.D., Stokes, C.R., Evans, D.J.A., 2014b. Increased channelization of subglacial drainage during deglaciation of the Laurentide ice sheet. Geology 42, 239–242. https://doi.org/10.1130/G35092.1.

Stroeven, A.P., Hättestrand, C., Kleman, J., Heyman, J., Fabel, D., Fredin, O., Goodfellow, B.W., Harbor, J.M., Jansen, J.D., Olsen, L., Caffee, M.W., Fink, D., Lundqvist, J., Rosqvist, G.C., Strömberg, B., Jansson, K.N., 2016. Deglaciation of Fennoscandia. Quat. Sci. Rev. 147, 91–121. https://doi.org/10.1016/j.quascirev.2015.09.016.